

## Numerical Investigation of the Effects of Channel Cross Section Shape on the Tubular PEMFC Performance

Open  
Access

Mohammed Abdallah<sup>1,\*</sup>, Ben Moussa Hocine<sup>1</sup>, Tamerabet Monsaf<sup>1</sup>, Sahli Youcef<sup>1,2</sup>

<sup>1</sup> Department of Mechanical engineering, Faculty of technology, University of Batna 2, Algeria

<sup>2</sup> Unité de Recherche en Energies Renouvelables en Milieu Saharien, URERMS, Centre de Développement des Energies Renouvelables, CDER, 01000 ADRAR, Algeria

### ARTICLE INFO

### ABSTRACT

#### Article history:

Received 21 September 2019

Received in revised form 3 December 2019

Accepted 5 December 2019

Available online 26 February 2020

In the present study, a novel tubular proton exchange membrane fuel cell with a twisted flow field is designed to investigate the effect of the channel cross section shapes on the transfer and consumption of reactants and cell performance. Comparisons between three different configurations: rectangular, trapezoidal and triangular cross sections are realized. A complete three-dimensional, isothermal, unsteady and single-phase model is employed. The finite volume method in the cylindrical coordinates is used to discretize the continuity, momentum and species conservation equations. A FORTRAN program is developed to resolve the discretized equations system. The velocity, reactants and water distributions are obtained for the three studied cross sections. The results establish that the triangular configuration shows the best performance relative to the trapezoidal and rectangular cross-sections, this configuration increases strongly in the flow velocity of reactants, enhancing water evacuation process and reactant consumptions. The rectangular cross section has the worst cell performance.

#### Keywords:

Channel cross section; twisted flow field;  
tubular PEMFC; reactants consumption;  
finite volume method

Copyright © 2020 PENERBIT AKADEMIA BARU - All rights reserved

## 1. Introduction

Fuel cells convert the chemical energy of a fuel directly into electrical energy with water production. They have the potential to reduce the energy use, pollutant emissions and dependence on fossil fuels [1-2]. The Proton exchange membrane fuel cell (PEMFC) is one of the most important types. Many factors influence the performance of the PEMFC, such as the operating conditions and the flow field design. The modification of the flow field dimensions and configurations such as the length, width and depth of the channel as well as its cross section form can be enhance the transport process of reactants through the catalyst layers, which can improve cell performance. Several numerical works have been developed in the main purpose of dealing with the complexity of the PEMFC phenomena that cannot be studied experimentally, and to improve the cell efficiency by

\* Corresponding author.

E-mail address: [a.mohammedi@univ-batna2.dz](mailto:a.mohammedi@univ-batna2.dz) (Mohammed Abdallah)

optimizing the channel configuration [3- 8]. Different designs of flow channel configurations have been proposed, including pins, meshes, integrated channels, Cascade channels, straight channels, serpentine and Interdigitated channels [3-4]. The fuel cell performance can be enhanced by using partial blockage of the flow along the channels [9]. Different types of blocks with profile shapes, square, semicircle and trapezoid, were used. It is confirmed that the influence of channel indentation increases the electrical current produced compared with the no-dent; also known as the base case. Besides, channel indentation causes a pressure drop along the dented channels [10]. Another parameter that can affect the cell performance is the channel cross section's shape. Dewan Hasan Ahmed *et al.*, [11] studied the channel cross section shape effect on a planar PEM fuel cell with straight single channels by using three different cross section shapes: parallelogram, trapezoidal and rectangular; they found that the channel with a rectangular cross section gives the highest cell voltages compared with the other two cross sections. Likewise, the trapezoidal cross section configuration improves the reactant distributions.

Wang *et al.*, [12] investigated numerically the effect of different cathode channel shapes namely; triangle, trapezoid, semicircle, and rectangular channel on the cell performance by using a three-dimensional, two-phase, and non-isothermal model of a planar PEM full cell; they found that triangle, trapezoid, and semicircle channel designs increase the flow velocity and enhance liquid water removal and reactants consumption. Compared with the rectangular channel design, these designs increase the current density and improve cell performance relatively. Shimpalee *et al.*, [13] used a commercial code to investigate the effect of channel cross section shape on the cell performance; that is, the channel's width/height ratio and the channel/rib width ratio. They found that the draft angle of the channel cross section affects strongly the performance of the PEMFC, and shows the biggest impact on uniformity in gas distributions, heat transport and pressure drop. The channel number influences on the PEM fuel cell performance has been investigated by Juarez-Robles *et al.*, [14]. They have introduced a numerical three-dimensional non-isothermal model of a planar PEM fuel cell with concentric spiral flow channels. They found that the use of a bipolar plate with four channels increases the current density produced, decreases the pressure drop and leads to a more uniform reactants distribution, which means the enhancement of the cell performance. In order to study the effects of the channel width, the number of turns of the spiral channel and the flow direction on the reactant consumptions in a planar PEM fuel cell, a three-dimensional model has been developed; it is found that the increase of the channel-rib width ratio improves the reactant distributions uniformity and enhances the cell performance. Increasing the number of turns of the spiral channel leads to similar results. Moreover, the advantage of using spiral channel design is the creation of a centrifugal force that enhances the cell performances when the reactants are injected by the outer side of the spiral channel [15]. To improve PEMFC power density, cost and durability, a tubular-shaped PEM fuel cell was compared with a conventional planar one. Regarding the temperature and reactants distribution, results showed that the tubular architecture shows better performance and a higher current density [16,17]. Khazaei and Ghazikhani [18] introduced a single-phase, non-isothermal model for PEMFC with annular cross-section. They showed that increasing the number of connections between GDL and bipolar plates enhances the fuel cell performance and increases the current density. Akbar Mohammadi-Ahmar *et al.*, [19,20] used a three-dimensional model of a tubular PEMFC to study the effects of arrangement and number of membrane, and catalyst and gas diffusion layers on the cell performance. Using the same active area and input mass flow, a comparison was made for different arrangements of the tubular-shaped PEMFC. Results show that by increasing the number of layers, the consumption of reactants is remarkable, which means it enhances power production. Furthermore, a numerical simulation under a steady state and non-isothermal conditions was developed to improve the fuel cell performance by using different cross

sections for tubular PEMFC [21]; it is found that circular and square cross sections increase the current density and lead to more uniform reactants distribution, but this is not the case with octagonal cross section designs. Sierra *et al.*, [22] proposed cylindrical geometries with three flow fields namely: serpentine, interdigitated and straight channels to evaluate the performance in PEM fuel cell. Numerical results showed that the configuration with cylindrical channels reduces the pressure drop owing to the gradual reduction of the angle of the flow path. Therefore, it facilitates the ejection of liquid water from gas diffusion layers.

Innovative architectures and flow fields designs could enhance PEM fuel cell performance and reduce their cost. Hence, the tubular architecture is more advantageous than of the planar architecture according to several reasons: it results in more uniform reactant distributions, more uniform pressure applied to the MEA by the cathode and a greater cathode surface that increases the amount of oxygen reduction [16].

In the present study, which represents a continuation of our ones [23-31], a novel geometry of tubular PEM Fuel Cell with twisted channels is suggested. The effect of different channel cross-section shapes namely: rectangular, trapezoidal and triangular on the reactant consumptions are investigated to explore PEM Fuel Cell possible potential for being one of the best candidate configurations for the next generation of the PEM fuel cell productions.

## 2. Model Description

### 2.1 Physical Model

In this study, we used a single cell model, which consists of a membrane, an anode and a cathode superposed as three concentric tubular thin layers and two twisted flow channels on both sides of the tubular MEA (Membrane Electrode Assembly) as it is shown in Figure 1. The dimensions of each configuration are presented in Table 1. The catalyst layers are considered as thin interfaces between the membrane and electrodes. To study the effect of the channel cross section shape, we realized a comparison between three different configurations using rectangular, trapezoidal and triangular cross sections. The three cross section shapes proposed for PEMFC have the same active area and operation conditions. In addition, the cell's electrochemical properties are presented in Table 2.

**Table 1**

Channel cross section dimensions

Cross section geometry	Dimensions		
	A (mm)	B (mm)	C (mm)
Rectangular	1	1	1
Trapezoidal	1	1	0.5
Triangular	1	1	0

### 2.2 Model Assumptions

The used assumptions to carry out and complete the simulation of the proposed three-dimensional model are as follows: (i) flows in channels are supposed laminar. (ii) Inlet gas is an incompressible fluid. (iii) The system operates under the unsteady state condition. (iv) Water in channels and gas diffusion layers is considered as vapor. (v) Water is produced in the vapor state. (vi) Diffusion layers are homogeneous and isotropic. (vii) The membrane is fully humidified so that the ionic conductivity is constant.

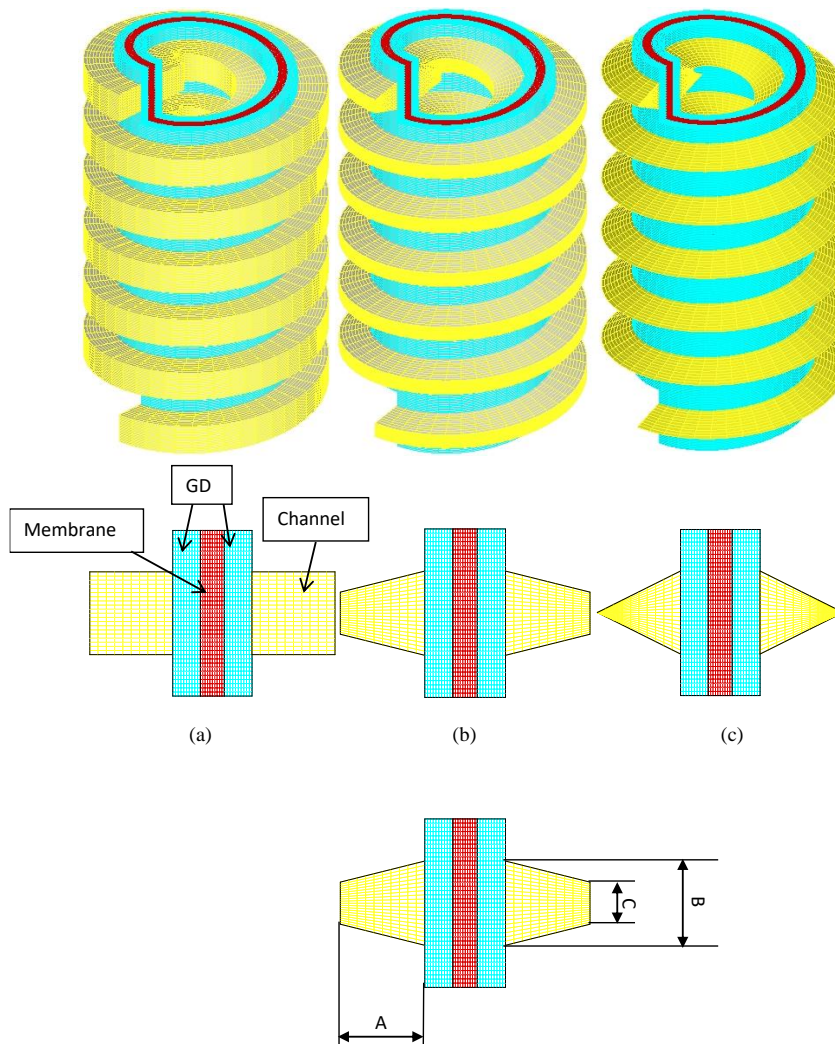


**Fig. 1.** Simulation domain for the three different studied cross-sections: (a) rectangular; (b) trapezoidal; (c) triangular

**Table 2**  
 Electrochemical properties [13]

Property	Value
GDL and catalyst conductivity	$53 \Omega^{-1}/m$
GDL porosity	0.4
Catalyst porosity	0.4
Concentration exp. (anode)	0.5
Concentration exp. (cathode)	1
Transfer coefficient (anode)	2
Ref. current density (anode)	$10^9 A/m^3$
Transfer coefficient (cathode)	2
Ref. current density (cathode)	$3 \times 10^5 A/m^3$
Hydrogen reference diffusivity	$1.1 \times 10^{-4} m^2/s$
Oxygen reference diffusivity	$3.2 \times 10^{-5} m^2/s$
Water reference diffusivity	$7.35 \times 10^{-5} m^2/s$
Permeability	$2 \times 10^{-10} m^2$

## 2.3 Governing Equations

The governing equations of continuity, momentum and mass conservation represent the transport phenomena occurring inside a PEM fuel cell. A three-dimensional isothermal unsteady model in cylindrical coordinates was applied to describe the different phenomena.

### 2.3.1 Continuity equation

$$\frac{\partial(\rho u_r)}{\partial r} + \frac{1}{r} \frac{\partial(\rho u_\theta)}{\partial \theta} + \frac{\partial(\rho u_z)}{\partial z} = 0 \quad (1)$$

### 2.3.2 Momentum equations

Three-dimensional Navier-Stokes equations are resolved in cylindrical coordinates

$$\frac{\partial \varepsilon \rho u_r}{\partial t} + u_r \frac{\partial \varepsilon \rho u_r}{\partial r} + \frac{u_\theta}{r} \frac{\partial \varepsilon \rho u_r}{\partial \theta} + u_z \frac{\partial \varepsilon \rho u_r}{\partial z} = \frac{1}{r} \frac{\partial}{\partial r} \left( r \varepsilon \mu \frac{\partial u_r}{\partial r} \right) + \frac{1}{r} \frac{\partial}{\partial \theta} \left( \varepsilon \mu \frac{1}{r} \frac{\partial u_r}{\partial \theta} \right) + \frac{\partial}{\partial z} \left( \varepsilon \mu \frac{\partial u_r}{\partial z} \right) + S_r \quad (2)$$

$$\frac{\partial \varepsilon \rho u_\theta}{\partial t} + u_r \frac{\partial \varepsilon \rho u_\theta}{\partial r} + \frac{u_\theta}{r} \frac{\partial \varepsilon \rho u_\theta}{\partial \theta} + u_z \frac{\partial \varepsilon \rho u_\theta}{\partial z} = \frac{1}{r} \frac{\partial}{\partial r} \left( r \varepsilon \mu \frac{\partial u_\theta}{\partial r} \right) + \frac{1}{r} \frac{\partial}{\partial \theta} \left( \varepsilon \mu \frac{1}{r} \frac{\partial u_\theta}{\partial \theta} \right) + \frac{\partial}{\partial z} \left( \varepsilon \mu \frac{\partial u_\theta}{\partial z} \right) + S_\theta \quad (3)$$

$$\frac{\partial \varepsilon \rho u_z}{\partial t} + u_r \frac{\partial \varepsilon \rho u_z}{\partial r} + \frac{u_\theta}{r} \frac{\partial \varepsilon \rho u_z}{\partial \theta} + u_z \frac{\partial \varepsilon \rho u_z}{\partial z} = \frac{1}{r} \frac{\partial}{\partial r} \left( r \varepsilon \mu \frac{\partial u_z}{\partial r} \right) + \frac{1}{r} \frac{\partial}{\partial \theta} \left( \varepsilon \mu \frac{1}{r} \frac{\partial u_z}{\partial \theta} \right) + \frac{\partial}{\partial z} \left( \varepsilon \mu \frac{\partial u_z}{\partial z} \right) + S_z \quad (4)$$

where  $S_r$ ,  $S_\theta$ , and  $S_z$  represent the source term. It is expressed for each velocity component as follows

$$S_r = - \left( \frac{\mu}{r^2} + \frac{\varepsilon^2 \mu}{k} \right) u_r - \left( \frac{\varepsilon \rho u_\theta^2}{r} + \varepsilon \frac{\partial P}{\partial r} + \mu \varepsilon \frac{2}{r^2} \frac{\partial u_\theta}{\partial \theta} \right) \quad (5)$$

$$S_\theta = - \left( \frac{\varepsilon \rho u_r}{r} + \frac{\mu \varepsilon}{r^2} + \frac{\varepsilon^2 \mu}{k} \right) u_\theta - \left( \varepsilon \frac{\partial P}{r \partial \theta} + \mu \varepsilon \frac{2}{r^2} \frac{\partial u_r}{\partial \theta} \right) \quad (6)$$

$$S_z = - \frac{\varepsilon^2 \mu}{k} u_z - \varepsilon \frac{\partial P}{\partial z} \quad (7)$$

### 2.3.3 Species conservation equation

The equation of species represents the mass conservation for each individual species of a gas

$$\frac{\partial \varepsilon C_k}{\partial t} + u_r \frac{\partial \varepsilon C_k}{\partial r} + \frac{u_\theta}{r} \frac{\partial \varepsilon C_k}{\partial \theta} + u_z \frac{\partial \varepsilon C_k}{\partial z} = \frac{1}{r} \frac{\partial}{\partial r} \left( r \varepsilon D_k \frac{\partial C_k}{\partial r} \right) + \frac{1}{r} \frac{\partial}{\partial \theta} \left( \varepsilon D_k \frac{1}{r} \frac{\partial C_k}{\partial \theta} \right) + \frac{\partial}{\partial z} \left( \varepsilon D_k \frac{\partial C_k}{\partial z} \right) + S_k \quad (8)$$

$S_k$ : the source term for the species k, which can be Oxygen, Hydrogen or Water. The diffusivities are corrected using the Bruggemann correction formula [8]

$$D_k^{ef} = D_k \varepsilon^{1.5} \quad (9)$$

$D_k^{ef}$  is the effective diffusivity of the species k,  $D_k$  is the diffusivity of the species k and  $\varepsilon$  is the layer's porosity. The diffusivity of oxygen, hydrogen and water are calculated using Eq. (10) [9,18]

$$D_k = D_k^0 \left( \frac{T}{T_0} \right)^{\frac{3}{2}} \left( \frac{P_0}{P} \right) \quad (10)$$

$D_k^0$  is the diffusivity of the species  $k$  at the reference temperature and pressure,  $T_0 = 300k$  and  $P_0 = 1 atm$ , respectively. The catalyst layer thickness is negligible: it can be considered as a thin interface between the membrane and electrodes [32]. At the cathode catalyst layer interface, the source terms for oxygen water are respectively given by

$$S_{O_2} = -\frac{j_c}{4F} \quad (11)$$

$$S_{H_2O} = \frac{j_c}{2F} \quad (12)$$

At the anode catalyst layer interface, the source term for hydrogen is given as

$$S_{H_2} = -\frac{j_a}{2F} \quad (13)$$

$F$  is the faraday number and  $j_a$  and  $j_c$  are the volumetric current density at the anode and the cathode respectively. The volumetric current density can be modeled by the Butlere-Volmer equation [15]

$$j_c = j_{0,c}^{ref} \left( \frac{C_{O_2}}{C_{O_2}^{ref}} \right)^{\gamma_{O_2}} \left( e^{\frac{\alpha_a F}{RT} \eta_{act,c}} + e^{-\frac{\alpha_c F}{RT} \eta_{act,c}} \right) \quad (14)$$

$$j_a = j_{0,a}^{ref} \left( \frac{C_{H_2}}{C_{H_2}^{ref}} \right)^{\gamma_{H_2}} \left( e^{\frac{\alpha_a F}{RT} \eta_{act,a}} + e^{-\frac{\alpha_c F}{RT} \eta_{act,a}} \right) \quad (15)$$

The cell potential is determined using the following formula

$$E_{cell} = E - \eta_{act} - \eta_{ohm} - \eta_{Diff} \quad (16)$$

The equilibrium potential is determined using the Nernst equation [16,33].

$$E = 1.229 - 0.85 \times 10^{-3}(T - 298.15) + 4.3085 \times 10^{-5}T \left[ \ln \left( P_{H_2} + \frac{1}{2} P_{O_2} \right) \right] \quad (17)$$

Activation overpotential is given by: [15,33,34]

$$\eta_{act} = -[\xi_1 + \xi_2 T + \xi_3 T \ln(C_{O_2}) + \xi_4 T \ln(i)] \quad (18)$$

where "i" is the current density and  $\xi_1$ ,  $\xi_2$ ,  $\xi_3$  and  $\xi_4$  are parametric coefficients for each fuel cell model [15,34]

$$\begin{cases} \xi_1 = -0.948 \\ \xi_2 = 0.00286 + 0.0002 \ln(A_{MEA}) + 4.3 \cdot 10^{-5} \ln(C_{H_2}) \\ \xi_3 = 7.6 \cdot 10^{-5} \\ \xi_4 = -1.9310^{-4} \end{cases} \quad (19)$$

The membrane resistance, due to the ohmic overpotential produced by the hydrogen ions transport, is given by the following expression [15]

$$\eta_{ohm} = i \frac{\delta_m}{\sigma_m} \quad (20)$$

$\delta_m$  and  $\sigma_m$  are respectively the membrane thickness and conductivity, this last one is a function of water content and temperature, its local value is defined by the following empirical expression [18,22,35]

$$\sigma_m = [0.5139\lambda - 0.326] \exp \left[ 1268 \left( \frac{1}{303} - \frac{1}{T} \right) \right] \quad (21)$$

The water content  $\lambda$  is given by [12,14,18,22,35]

$$\begin{cases} \lambda = 0.043 + 17.10 a - 39.85 a^2 + 36.00 a^3 & \text{si } a \leq 1 \\ \lambda = 14.0 + 1.4(a - 1) & \text{si } a > 1 \end{cases} \quad (22)$$

The water activity  $a$  can be expressed as [9,15]

$$a = \frac{C_{H_2O} RT}{P_{sat}} \quad (23)$$

The saturation pressure of water vapor can be calculated by the following empirical equation [9,12,14,34-35]

$$\log_{10} P_{sat} = -2.1794 + 0.02953(T - 273.15) - 9.1837 \times 10^{-5} \times (T - 273.15)^2 + 1.4454 \times 10^{-7} \times (T - 273.15)^3 \quad (24)$$

Diffusion overpotentials are given by [16,34]

$$\eta_{Diff} = \frac{RT}{2F} \ln \left( 1 - \frac{i}{i_{max}} \right) \quad (25)$$

## 2.4 Initial and Boundary Conditions

### 2.4.1 Initial conditions

The stack is initially supposed empty (there is no reactant) while the initial concentrations of the different species are null. The velocity is initialized by a null value as

$$P_0 = u_{r,0} = u_{\theta,0} = u_{z,0} = C_{k0} = 0 \quad (26)$$

The boundary conditions are applied to all external borders of the computational domain.

### 2.4.2 Inlet conditions

Pressure, velocity and Species concentrations are imposed (Dirichlet condition) at the channel inlet and the flows of hydrogen and oxygen were fed in the same direction.

### 2.4.3 Output conditions

At the flow channels outlet, we assume that the gradient of all variables in the flow direction are null (Neumann condition).

$$\frac{\partial u_\theta}{r\partial\theta} = \frac{\partial u_r}{r\partial\theta} = \frac{\partial u_z}{r\partial\theta} = \frac{\partial P}{r\partial\theta} = \frac{\partial C_{O_2}}{r\partial\theta} = \frac{\partial C_{H_2}}{r\partial\theta} = \frac{\partial C_{H_2O}}{r\partial\theta} = 0 \quad (27)$$

### 2.4.4 External surfaces

The species concentrations gradient is null which means there is no matter flux through the external surfaces. The velocities on the external surfaces are null because of the condition of adhesion to the wall.

### 2.5 Numerical method

A FORTRAN program has been developed to construct the computational domain geometry, to create the mesh and to solve the problem governing equations. The essential steps of the simulation program are shown in Figure 2.

To ensure that the solutions are independent of the grid size, we tested several grids with different sizes, as shown in Figure 4. A grid with 590000 cells showed an error less than 1.5% in the power density, which is the lowest error. This grid size is required to provide an acceptable solution of the problem.

The module responsible on the generation of geometry and mesh is illustrated in Figure 3.

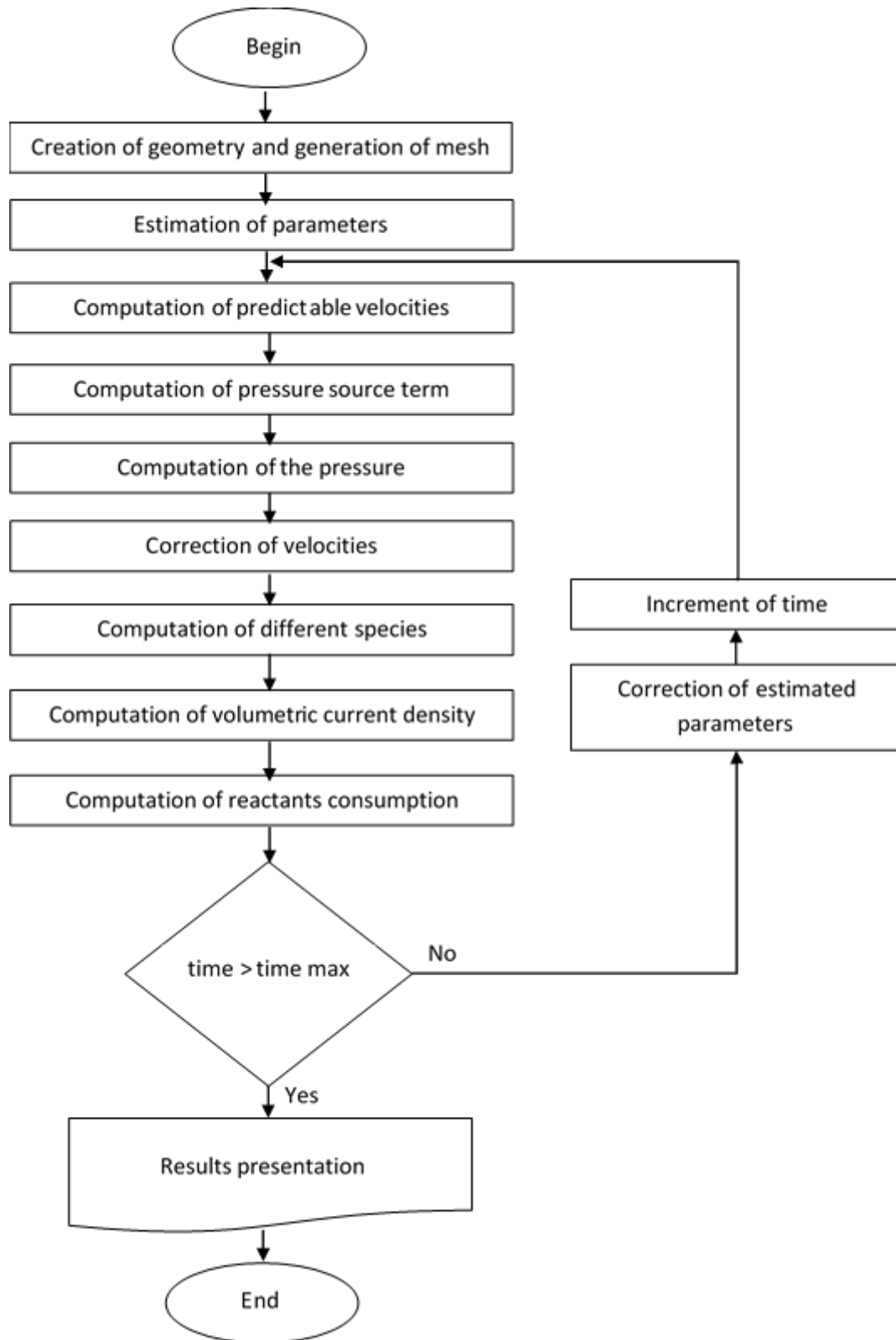
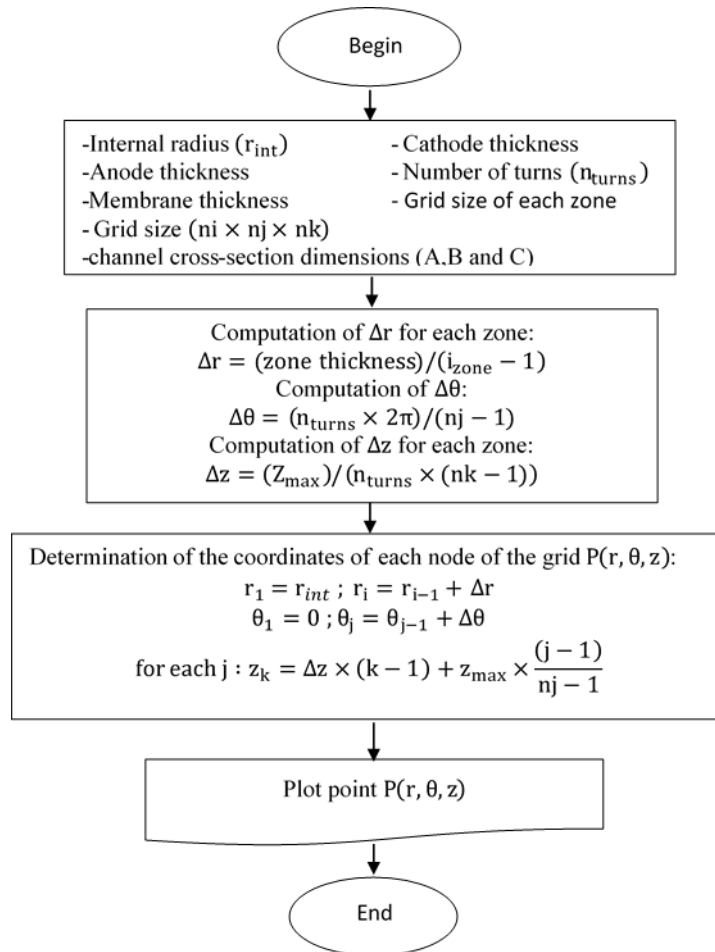
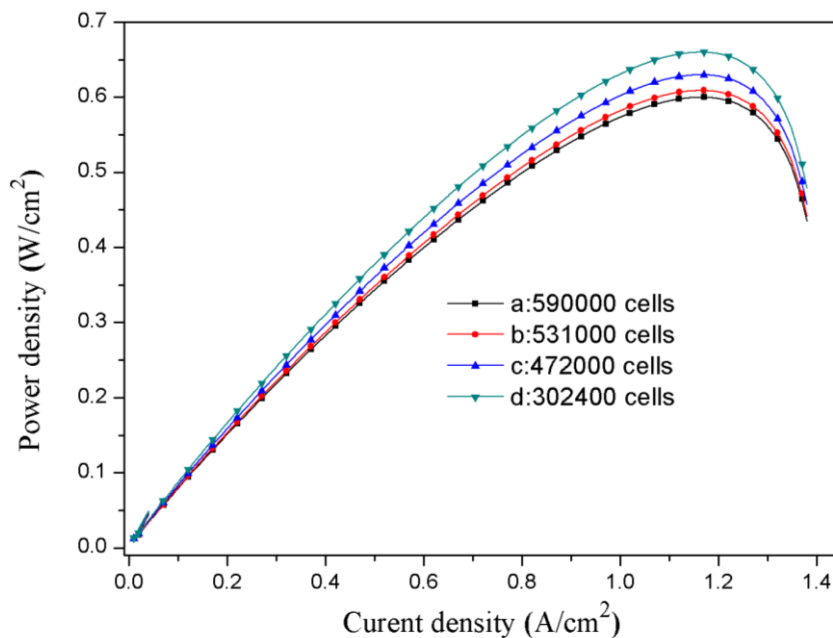


Fig. 2. Computational algorithm



**Fig. 3.** Main steps of the algorithm used to create geometry and mesh



**Fig. 4.** Mesh independency checking, a :30\*295 \*40 for the MEA and 20\*295 \*20 for channels, b :30\*295 \*36 for the MEA and 20\*295 \*18 for channels, c :30\*295 \*32 for the MEA and 20\*295 \*16 for channels, d :30\*295 \*28 for the MEA and 20\*295 \*14 for channels

The governing equations take the shape of the transport equation which can be written for function  $\phi$  as

$$\frac{\partial}{\partial t}(\epsilon_r \rho \phi) + \text{div}(\epsilon_r \rho u \phi) = \text{div}(\Gamma \text{grad}(\phi)) + S_\phi \quad (28)$$

The discretization of the conservation equations by the finite volume method in the cylindrical coordinates lead us to obtain a set of linear algebraic equations which needs to be solved. The conservation equations have been discretized in time over a finite number of intervals of constant length  $[t_n, t_n + \Delta t]$  According to an implicit scheme which is unconditionally stable. The power scheme has been chosen for the discretization of convective terms. This scheme has the advantage that it is less expensive than the exponential scheme, while reproducing its behavior. After a rearrangement of the formula (28), we have the final form

$$a_p \cdot \phi_P^{t+\Delta t} = a_w \cdot \phi_W^{t+\Delta t} + a_e \cdot \phi_E^{t+\Delta t} + a_s \cdot \phi_S^{t+\Delta t} + a_n \cdot \phi_N^{t+\Delta t} + a_b \cdot \phi_B^{t+\Delta t} + a_t \cdot \phi_T^t + a_p^0 \cdot \phi_p^{t+\Delta t} + S_u \cdot \Delta V \quad (29)$$

The problem of pressure-velocity coupling equations is solved by using the projection algorithm [36]. In order to reduce the dimensionality problem from three dimensions to one dimension, we applied the ADI method on the set of algebraic Eq. (29)

The ADI method consists of dividing each time step into three subintervals: from " $t$ " to " $t + \Delta t/3$ ", from " $t + \Delta t/3$ " to " $t + 2\Delta t/3$ " and from " $t + 2\Delta t/3$ " to " $t + \Delta t$ ". In each subinterval, one direction is implicit but the two other directions are explicit and the Eq. (29) can be written in each subinterval as [15]

First subinterval

$$-aw_{i,j,k} \phi_{i-1,j,k}^{t+\frac{1}{3}\Delta t} + ap_{i,j,k} \phi_{i,j,k}^{t+\frac{1}{3}\Delta t} - ae_{i,j,k} \phi_{i,j+1,k}^{t+\frac{1}{3}\Delta t} = +as_{i,j,k} \phi_{i,j-1,k}^t + an_{i,j,k} \phi_{i,j+1,k}^t + ab_{i,j,k} \phi_{i,j,k-1}^t + at_{i,j,k} \phi_{i,j,k+1}^t + ap_{i,j,k}^0 \phi_{i,i,k}^t + S_{P,i,j,k} \Delta V \quad (30)$$

Second subinterval

The discretization will be implicit in the tangential direction  $\theta$  and explicit in the other two directions

$$-as_{i,j,k} \phi_{i,j-1,k}^{t+\frac{2}{3}\Delta t} + ap_{i,j,k} \phi_{i,j,k}^{t+\frac{2}{3}\Delta t} - an_{i,j,k} \phi_{i,j+1,k}^{t+\frac{2}{3}\Delta t} = +aw_{i,j,k} \phi_{i-1,j,k}^{t+\frac{1}{3}\Delta t} + ae_{i,j,k} \phi_{i+1,j,k}^{t+\frac{1}{3}\Delta t} + ab_{i,j,k} \phi_{i,j,k-1}^{t+\frac{1}{3}\Delta t} + at_{i,j,k} \phi_{i,j,k+1}^{t+\frac{1}{3}\Delta t} + ap_{i,j,k}^0 \phi_{i,i,k}^{t+\frac{1}{3}\Delta t} + S_{P,i,j,k} \Delta V \quad (31)$$

Third subinterval

The discretization will be implicit in the tangential direction  $z$  and explicit in the other two directions

$$-ab_{i,j,k} \phi_{i,j,k-1}^{t+\Delta t} + ap_{i,j,k} \phi_{i,j,k}^{t+\Delta t} - at_{i,j,k} \phi_{i,j,k+1}^{t+\frac{2}{3}\Delta t} = +aw_{i,j,k} \phi_{i-1,j,k}^{t+\frac{2}{3}\Delta t} + ae_{i,j,k} \phi_{i+1,j,k}^{t+\frac{2}{3}\Delta t} + as_{i,j,k} \phi_{i,j-1,k}^{t+\frac{2}{3}\Delta t} + an_{i,j,k} \phi_{i,j+1,k}^{t+\frac{2}{3}\Delta t} + ap_{i,j,k}^0 \phi_{i,i,k}^{t+\frac{2}{3}\Delta t} + S_{P,i,j,k} \Delta V \quad (32)$$

Each of the Eq. (30), (31) and (32) presents a one-dimensional problem which can be resolved using the tridiagonal matrix algorithm. For every step of time, the pressure equation takes the form of Poisson equation, so we resolved it using the iterative method of Gauss-Seidel.

### 3. Results and Discussion

In the aim to define the effect of the channel cross section on the reactant consumptions, the simulation results, for different used configurations, will be presented and discussed in this section. The profiles of velocity, concentration of oxygen, hydrogen and water, as well as, the polarization curves will be presented.

For validating the present work, the obtained results for the PEM fuel cell polarization curve was compared with experimental data of Wang *et al.*, [37] which is presented in Figure 5. However, the results indicate a slight deviation from the experiments but show a very good agreement. Hence, the three-dimensional numerical model can be used to accurately analyze the effects of the cross-sectional channel shape on the tubular PEM fuel cell performance.

This behavior indicates that the PEMFC test system does not produce liquid water even at low operating voltage, which confirms that the numerical model with the assumption of a single water phase predicts well the transport phenomena inside the cell [15].

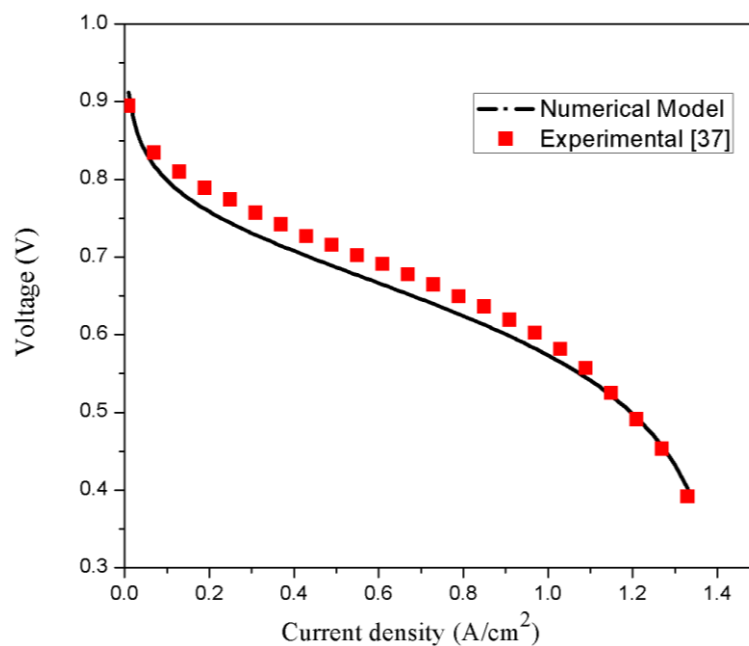


**Fig. 5.** Polarization curve of the Comparison between the numerical model and the experimental data

#### 3.1 Velocity Distribution

Figure 6 presents the velocity contours obtained by using three different cross-sections. These configurations are supplied with the same flow rate. We can observe that the maximum velocity distribution in the rectangular cross section is all along the center of the channel and maintains a

laminar profile. While in the case of the triangular cross section, the maximum velocity is located closely to the channel-GDL interface due to the dead zone developed at the summit of the triangular cross-section and to the suppression faced on the two side walls. Similarly, the replacement of the rectangular cross section by the trapezoidal one engenders a displacement of the maximum velocity position in the same direction as in the triangular configuration; the trapezoidal cross section shape is an intermediate configuration between the rectangular and triangular ones. We also note that the rectangular cross section seem to show the largest channel cross sectional area and the least maximal velocity, which can affect the reactant distributions and consumption.

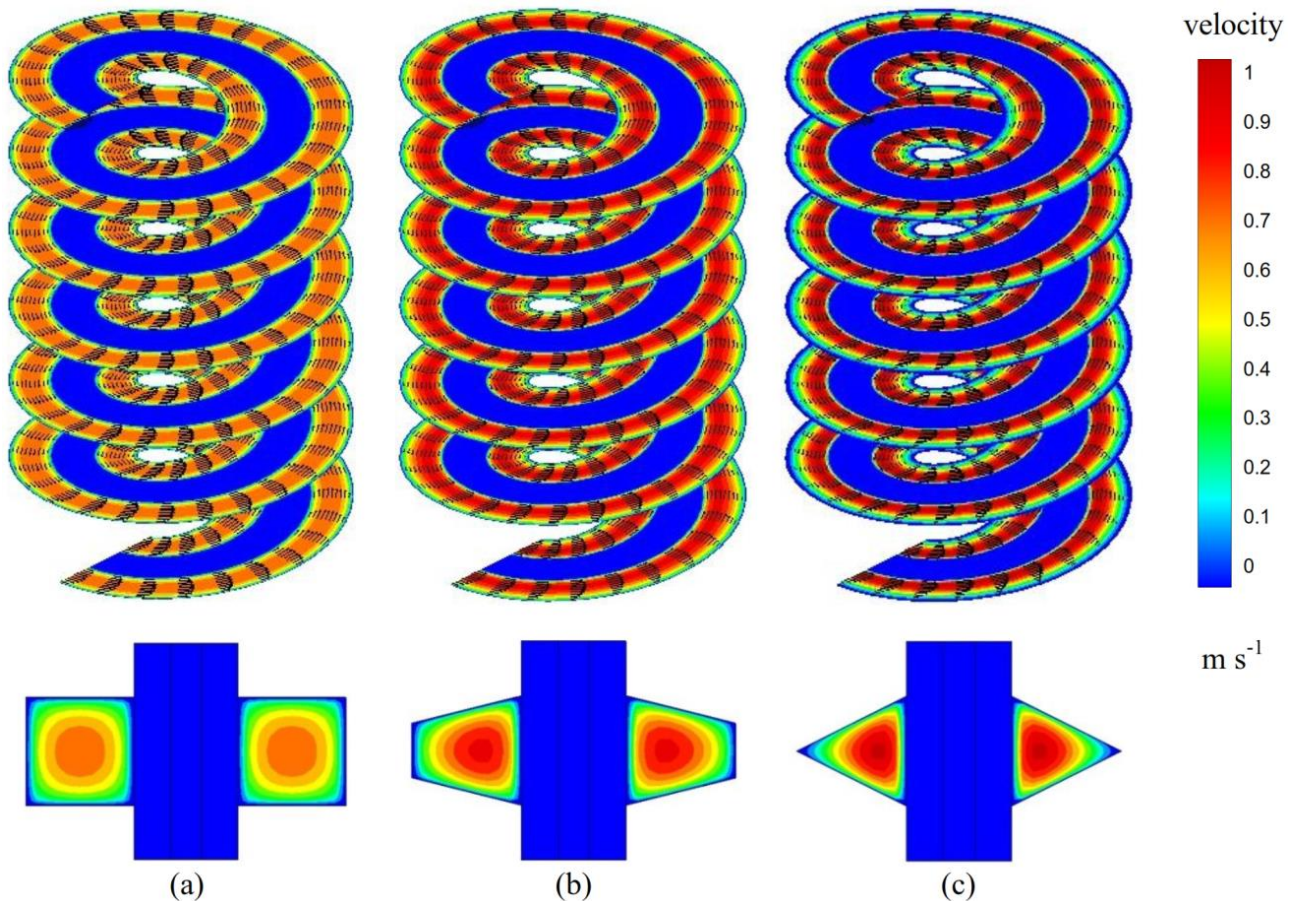


**Fig. 6.** Velocity distribution along the twisted channels: (a) rectangular, (b) trapezoidal, (c) triangular

### 3.2 Reactants Distribution

The hydrogen and oxygen distributions are respectively presented in Figure 7 and 8 for different configurations. As shown, the gases concentrations decrease along channels from the inlet to the outlet due to the reactant consumptions at the catalyst layer. In order to study the effect of the channel cross-section on the reactant consumptions, we take the rectangular one as a reference configuration. The replacement of this configuration by the trapezoidal one decreases the channel cross-section area and increases the flow velocity (in order to conserve the flow rate), which enhances the mass transfer process; more reactants are seeped to the gas diffusion layers and consumed at the catalyst ones. The enhancement of electrochemical rate increases the current density production and improves the cell performance as it is shown in Figure 10. The triangular configuration shows the best performance; the dead zone at the summit of the triangular channel acts as an obstacle which forces the flow to directed to the GDL across-which the reactants will

penetrate towards the catalyst layer. Hence, the conservation of the inlet flow rate and the area of the contact surface between the channel and the GDL have allowed us to conclude that the smaller channel cross-section will engender a higher velocity which will increase the seepage of reactants into the GDL enhancing the cell performance.

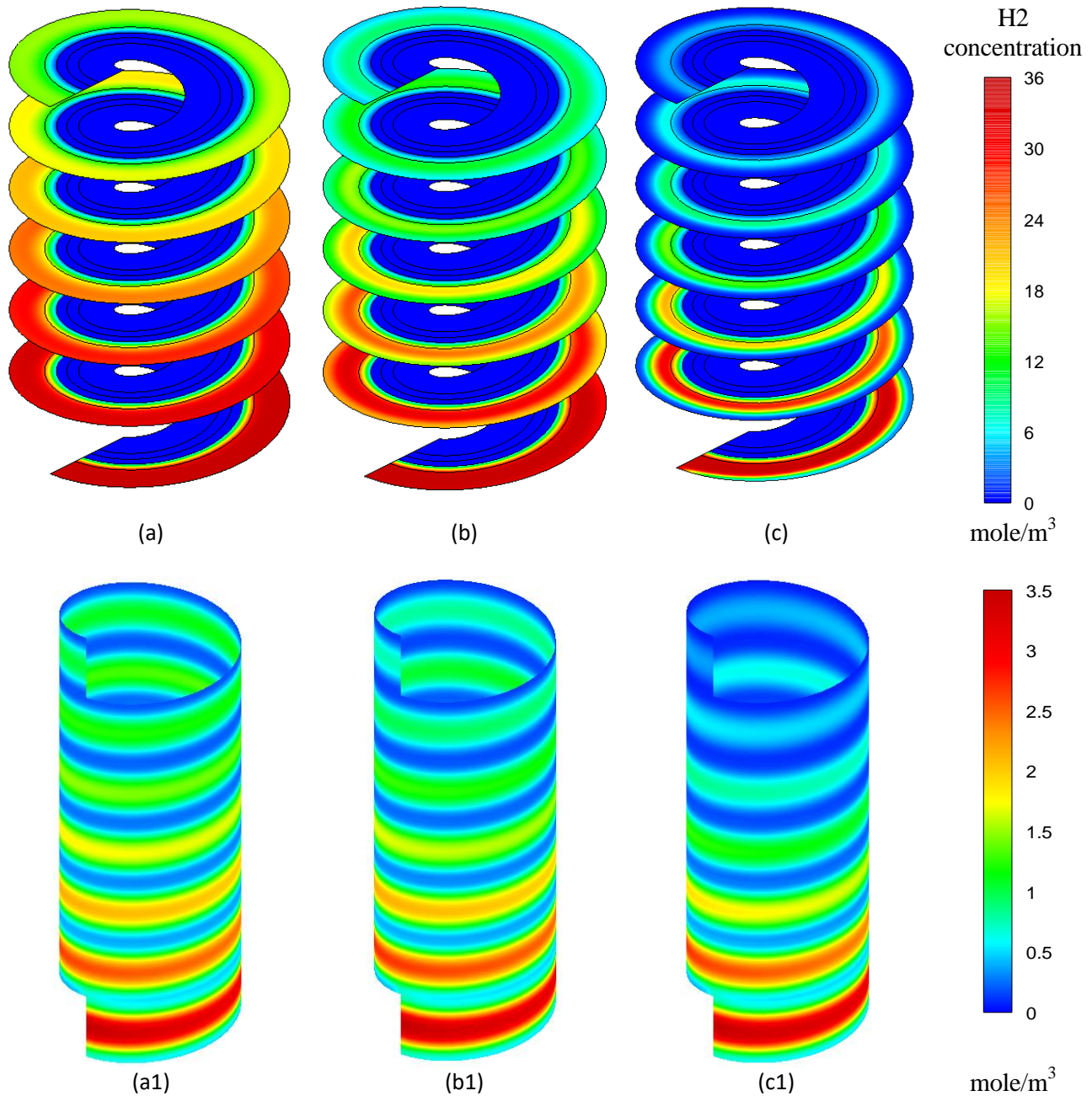


**Fig. 7.** Hydrogen concentration distribution along the twisted path: (a), (b) and (c) in the entire cell, (a1), (b1) and (c1) in the cathode CL/GDL interface

### 3.3 Water Distributions

The study of water concentration and distribution is required in order to avoid, at the same time, drying and submersion of the membrane and to ensure the proper functioning of the cell. The detailed distribution of water molar concentration in the cell is shown in Figure 9. As it is seen, water distribution contours in the anode and cathode for three cross section shapes (rectangular,

trapezoidal and triangular) in tubular geometry. Water is produced at the catalytic layer on the cathode side, where it can be seen that its concentration reaches maximal values. The concentration of water gradually decreases away from this layer, which engenders the water transfer by diffusion in this direction. The water produced at the cathode is divided into two parts. The first part passes through the membrane and the diffusion layer to the anode channel and the second part passes through the GDL to the cathode channel. Water in channels is carried by the convective forces in the flow direction and is ejected outward; that is the reason why water concentration in channels is gradually increasing from the inlet to the outlet, in which the maximal concentration of water in this zone is observed (Figure 9 (a2), (b2) and (c2)).

Water concentration in the cathode side is greater than that in the anode side because of the water generation on the cathode side and the membrane low permeability. Compared with the rectangular and trapezoidal configurations, the triangular cross section has the maximum value of water distribution in the MEA due to the high consumption rate, which decreases the furthest it gets into the twisted path. As shown in Figure 6, the triangular cross section has the most important velocity, which generates the most important convective force and enhances the water evacuation process; while the rectangular cross section provides more water distribution along the channel, which means that water is not removed but is accumulated in the cell parts. Hence, reduces the cell performance making the rectangular cross section the worst channel configuration performance wise. In brief, these novel tubular geometries considerably affect the water generation and its distribution along the cell.

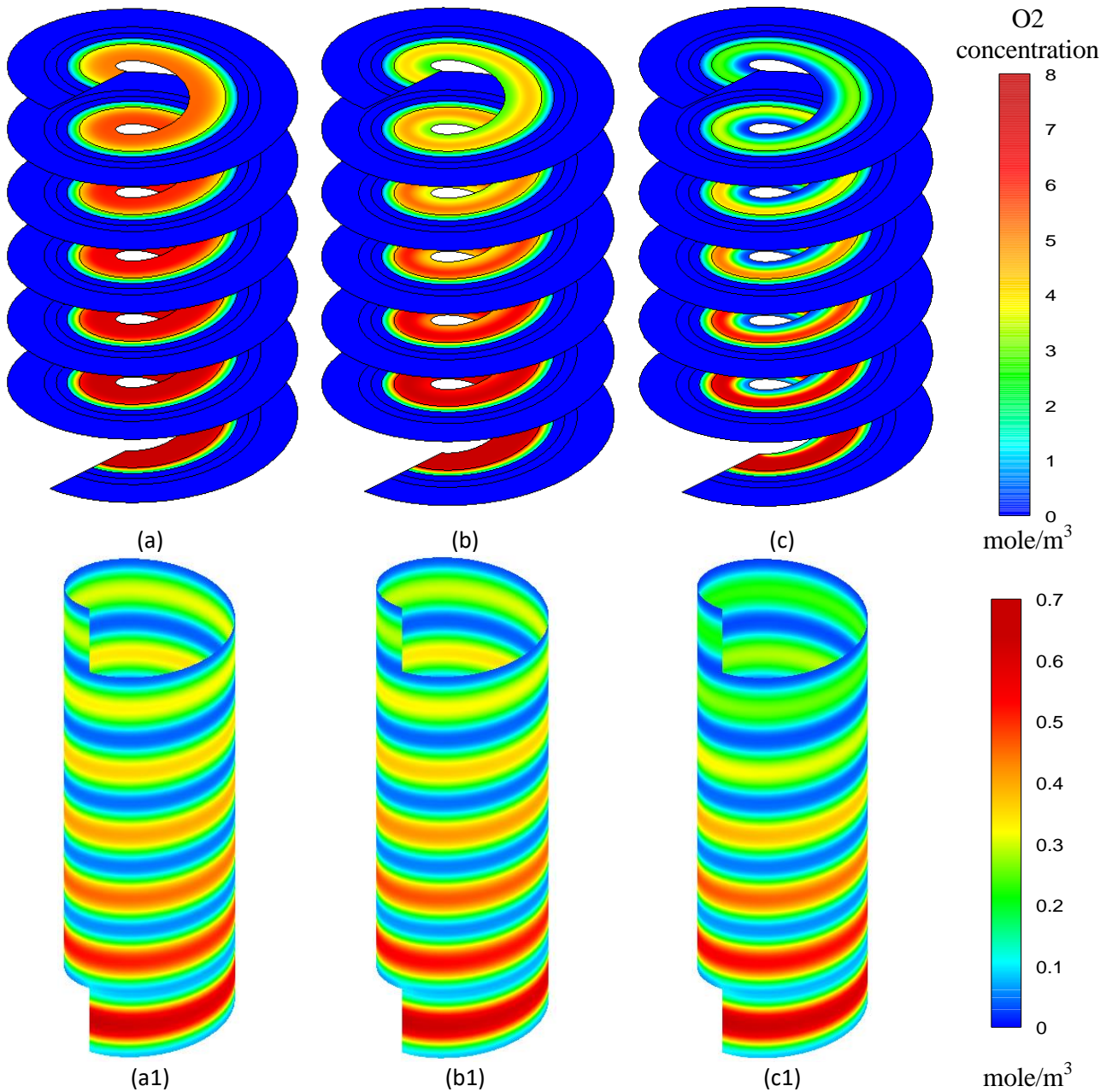


**Fig. 8.** Oxygen concentration distribution along the twisted path: (a), (b) and (c) in the entire cell, (a1), (b1) and (c1) in the cathode CL/GDL interface

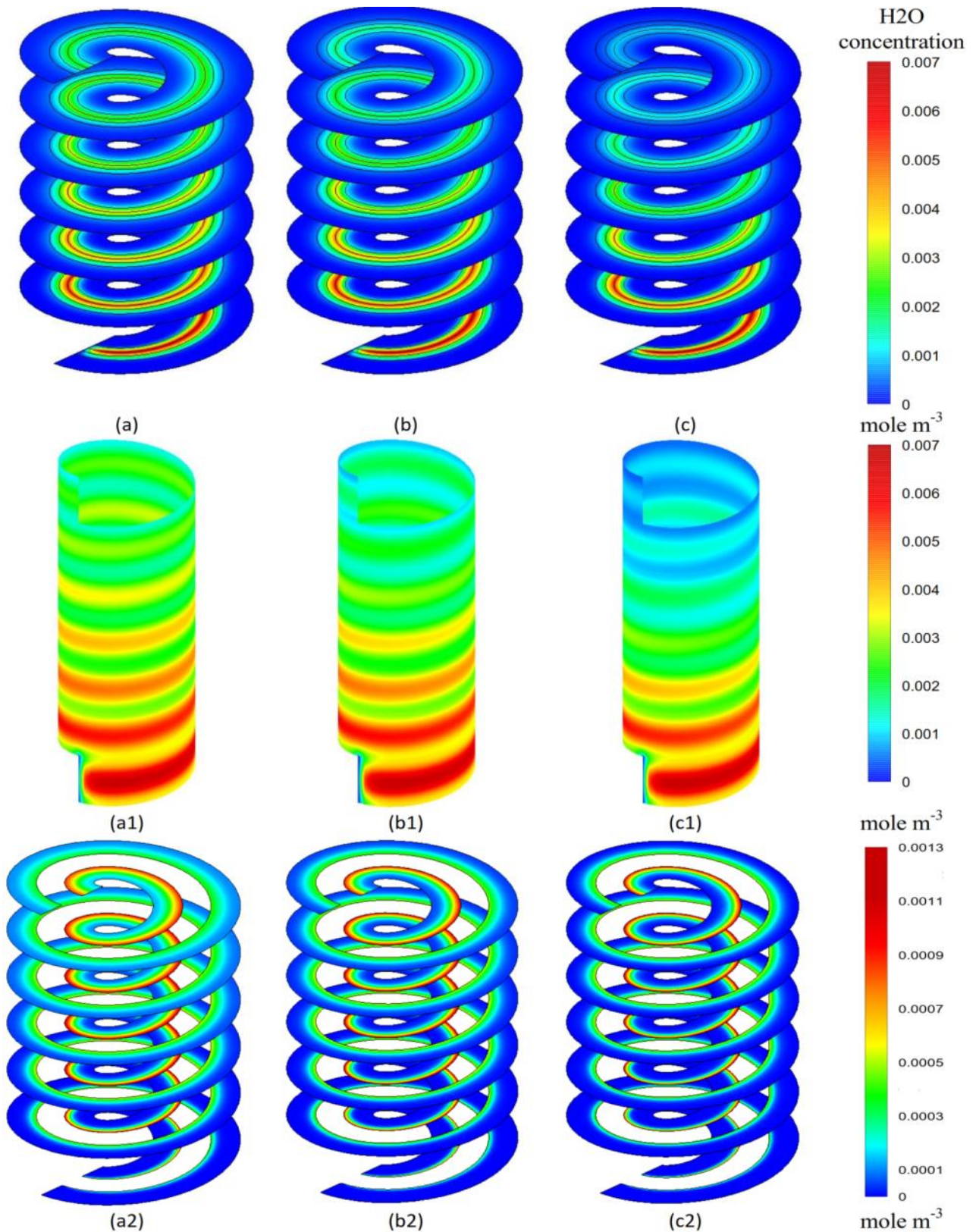


**Fig. 9.** Water concentration distributions. (a), (b) and (c): in the entire of cell, (a1), (b1) and (c1): at the cathode CL/GDL interface, (a2), (b2) and (c2): in channels

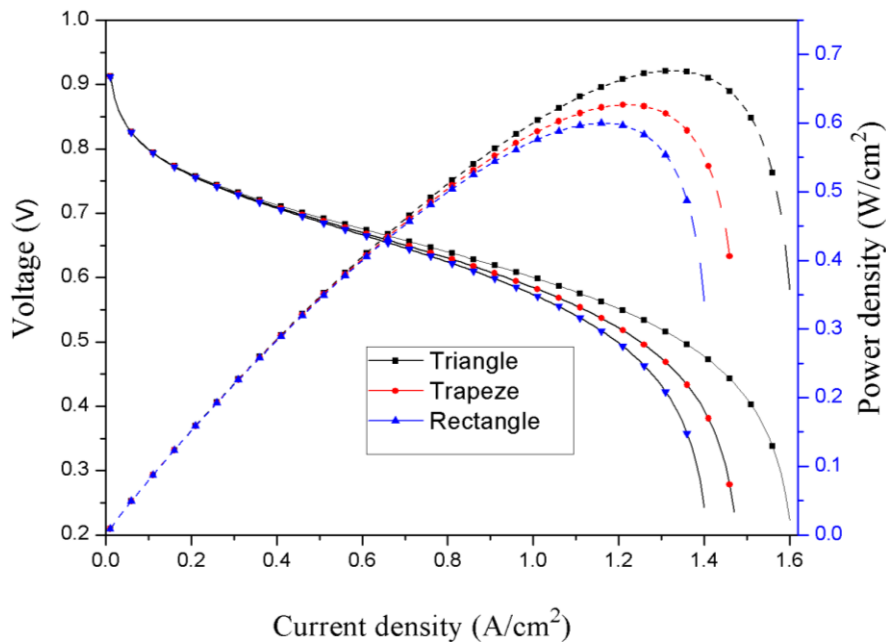


**Fig. 10.** Polarization curve for the three different cross sections.  
(tension: ——— ; power density: - - - - - .)

#### 4. Conclusion

In the present work, a software program using FORTRAN language was developed to investigate the effect of using different channel cross-section shapes on the velocity distribution, the reactant consumptions and the water generation, as well as to evaluate the performance of a novel tubular PEM Fuel Cell. The finite volume method was used to discretize the conservation equations, under an unsteady state, in the different parts of the cell. Under the same inlet flow rate, the conclusions drawn from the analyses are

- i. Contours of reactants and velocity distributions revealed that the reactant consumptions using the triangular cross section is much higher compared to the other configurations.
- ii. With the largest channel cross-sectional area, the flow velocity in the rectangular cross-section is far less than the other configurations which affect directly the reactant distributions and consumption.
- iii. The cell performance is strongly dependent on channel cross-section shapes. Compared to the rectangular and trapezoidal channels configurations, the triangular one enhances significantly the water evacuation process that improves the cell performance. It is far better than trapezoidal and rectangular channel ones in terms of efficiency, uniformity of reactants distribution and water. Hence, the triangular cross-sectional configuration can be therefore considered as the basic design for the tubular PEMFCs new generation.

#### References

- [1] Wang, Yun, Ken S. Chen, Jeffrey Mishler, Sung Chan Cho, and Xavier Cordobes Adroher. "A review of polymer electrolyte membrane fuel cells: Technology, applications, and needs on fundamental research." *Applied energy* 88, no. 4 (2011): 981-1007.
- [2] Sabaruddin, Muhammad Firdaus, Norahim Ibrahim, and N. A. R. Rashid. "Stacked configuration effect on microbial fuel cell performances via acid red 27 dye biodecolourisation." *Journal of Advanced Research in Materials Science* 37, no. 1 (2017): 24-35.
- [3] Manso, A. P., F. F. Marzo, J. Barranco, X. Garikano, and M. Garmendia Mujika. "Influence of geometric parameters of the flow fields on the performance of a PEM fuel cell. A review." *International journal of hydrogen energy* 37, no. 20 (2012): 15256-15287.

- [4] Li, Xianguo, and Imran Sabir. "Review of bipolar plates in PEM fuel cells: Flow-field designs." *International journal of hydrogen energy* 30, no. 4 (2005): 359-371.
- [5] Kahraman, Huseyin, and Mehmet F. Orhan. "Flow field bipolar plates in a proton exchange membrane fuel cell: Analysis & modeling." *Energy Conversion and Management* 133 (2017): 363-384.
- [6] Shimpalee, S., S. Greenway, and J. W. Van Zee. "The impact of channel path length on PEMFC flow-field design." *Journal of Power Sources* 160, no. 1 (2006): 398-406.
- [7] Owejan, Jon P., T. A. Trabold, D. L. Jacobson, Muhammad Arif, and S. G. Kandlikar. "Effects of flow field and diffusion layer properties on water accumulation in a PEM fuel cell." *International Journal of Hydrogen Energy* 32, no. 17 (2007): 4489-4502.
- [8] Sun, Lan, Patrick H. Oosthuizen, and Kim B. McAuley. "A numerical study of channel-to-channel flow cross-over through the gas diffusion layer in a PEM-fuel-cell flow system using a serpentine channel with a trapezoidal cross-sectional shape." *International Journal of Thermal Sciences* 45, no. 10 (2006): 1021-1026.
- [9] Tiss, F., R. Chouikh, and A. Guizani. "A numerical investigation of reactant transport in a PEM fuel cell with partially blocked gas channels." *Energy conversion and management* 80 (2014): 32-38.
- [10] Ghanbarian, Asrin, and M. Jafar Kermani. "Enhancement of PEM fuel cell performance by flow channel indentation." *Energy Conversion and management* 110 (2016): 356-366.
- [11] Ahmed, Dewan Hasan, and Hyung Jin Sung. "Effects of channel geometrical configuration and shoulder width on PEMFC performance at high current density." *Journal of Power Sources* 162, no. 1 (2006): 327-339.
- [12] Wang, Xiao-Dong, Gui Lu, Yuan-Yuan Duan, and Duu-Jong Lee. "Numerical analysis on performances of polymer electrolyte membrane fuel cells with various cathode flow channel geometries." *International Journal of Hydrogen Energy* 37, no. 20 (2012): 15778-15786.
- [13] Shimpalee, Sirivatch, Visarn Lilavivat, John W. Van Zee, Heather McCrabb, and Alonso Lozano-Morales. "Understanding the effect of channel tolerances on performance of PEMFCs." *International Journal of Hydrogen Energy* 36, no. 19 (2011): 12512-12523.
- [14] Juarez-Robles, Daniel, Abel Hernandez-Guerrero, Bladimir Ramos-Alvarado, Francisco Elizalde-Blancas, and Cesar E. Damian-Ascencio. "Multiple concentric spirals for the flow field of a proton exchange membrane fuel cell." *Journal of Power Sources* 196, no. 19 (2011): 8019-8030.
- [15] Monsaf, Tamerabet, Ben Moussa Hocine, Sahli Youcef, and Mohammedi Abdallah. "Unsteady three-dimensional numerical study of mass transfer in PEM fuel cell with spiral flow field." *International Journal of Hydrogen Energy* 42, no. 2 (2017): 1237-1251.
- [16] Al-Baghdadi, Maher AR Sadiq. "Studying the effect of material parameters on cell performance of tubular-shaped PEM fuel cell." *Energy conversion and management* 49, no. 11 (2008): 2986-2996.
- [17] Pourmahmoud, Nader, Hamidreza Sadeghifar, and Ashkan Torkavannejad. "A novel, state-of-the-art tubular architecture for polymer electrolyte membrane fuel cells: Performance enhancement, size and cost reduction." *International Journal of Heat and Mass Transfer* 108 (2017): 577-584.
- [18] Khazaei, Iman, and Mohsen Ghazikhani. "Performance improvement of proton exchange membrane fuel cell by using annular shaped geometry." *Journal of Power Sources* 196, no. 5 (2011): 2661-2668.
- [19] Mohammadi-Ahmar, Akbar, Behzad Osanloo, Ali Solati, and Jalal Ghasemi. "Performance improvement of the circular tubular PEMFC by using different architectures and number of layers." *Energy conversion and management* 128 (2016): 238-249.
- [20] Osanloo, Behzad, Akbar Mohammadi-Ahmar, and Ali Solati. "A numerical analysis on the effect of different architectures of membrane, CL and GDL layers on the power and reactant transportation in the square tubular PEMFC." *International Journal of Hydrogen Energy* 41, no. 25 (2016): 10844-10853.
- [21] Torkavannejad, Ashkan, Hamidreza Sadeghifar, Nader Pourmahmoud, and Farzin Ramin. "Novel architectures of polymer electrolyte membrane fuel cells: efficiency enhancement and cost reduction." *International Journal of Hydrogen Energy* 40, no. 36 (2015): 12466-12477.
- [22] Sierra, J. M., S. J. Figueroa-Ramírez, S. E. Díaz, J. Vargas, and P. J. Sebastian. "Numerical evaluation of a PEM fuel cell with conventional flow fields adapted to tubular plates." *International Journal of Hydrogen Energy* 39, no. 29 (2014): 16694-16705.
- [23] Laribi, Slimane, Khaled Mammar, Youcef Sahli, and Khaled Koussa. "Air supply temperature impact on the PEMFC impedance." *Journal of Energy Storage* 17 (2018): 327-335.
- [24] Abdenebi, Hafsa, Bariza Zitouni, Hocine Ben Moussa, Djamel Haddad, Hadda Zitouni, and Youcef Sahli. "Inlet methane temperature effect at a planar SOFC thermal field under direct internal reforming condition." In *Progress in Clean Energy, Volume 2*, pp. 567-581. Springer, Cham, 2015.
- [25] Laribi, Slimane, Khaled Mammar, Youcef Sahli, and Khaled Koussa. "Analysis and diagnosis of PEM fuel cell failure modes (flooding & drying) across the physical parameters of electrochemical impedance model: Using neural networks method." *Sustainable Energy Technologies and Assessments* 34 (2019): 35-42.

- [26] Laribi, Slimane, Khaled Mammar, Messaoud Hamouda, and Youcef Sahli. "Impedance model for diagnosis of water management in fuel cells using artificial neural networks methodology." *International Journal of Hydrogen Energy* 41, no. 38 (2016): 17093-17101.
- [27] Sahli, Youcef, Bariza Zitouni, Hocine Ben Moussa, and Hafsia Abdenebi. "Three-Dimensional Numerical Study of the Heat Transfer on The Planar Solid Oxide Fuel Cell: Joules Effect." In *Progress in Clean Energy, Volume 1*, pp. 449-461. Springer, Cham, 2015.
- [28] Sahli, Y., B. Zitouni, and H. Benmoussa. "Etude numérique tridimensionnelle de l'effet de la température d'entrée des gaz sur la production de chaleur dans une pile à combustible SOFC planaire." *Revue des Energies Renouvelables* 21, no. 2 (2018): 173-180.
- [29] Sahli, Youcef, Hocine Ben Moussa, and Bariza Zitouni. "Optimization study of the produced electric power by SOFCs." *International Journal of Hydrogen Energy* 44, no. 39 (2019): 22445-22454.
- [30] Sahli, Youcef, Bariza Zitouni, and Hocine Ben-Moussa. "Solid oxide fuel cell thermodynamic study." *Çankaya Üniversitesi Bilim ve Mühendislik Dergisi* 14, no. 2 (2017).
- [31] Sahli, Youcef, Bariza Zitouni, and Hocine Ben-Moussa. "Thermodynamic optimization of the solid oxyde fuel cell electric power." *UPB Sci Bull Ser B Chem Mater Sci* 80, no. 2 (2018): 159-170.
- [32] Al-Baghdadi, Maher AR Sadiq. "Performance comparison between airflow-channel and ambient air-breathing PEM fuel cells using three-dimensional computational fluid dynamics models." *Renewable Energy* 34, no. 7 (2009): 1812-1824.
- [33] Al-Baghdadi, Maher AR Sadiq. "Modelling of proton exchange membrane fuel cell performance based on semi-empirical equations." *Renewable Energy* 30, no. 10 (2005): 1587-1599.
- [34] Haddad, Djamel, Kafia Oulmi, Hocine Benmoussa, Zeroual Aouachria, and Nouredine Bourmada. "Transport phenomena effect on the performance of proton exchange membrane fuel cell (PEMFC)." *International Journal of Hydrogen Energy* 38, no. 20 (2013): 8550-8556.
- [35] Springer, Thomas E., T. A. Zawodzinski, and Shimshon Gottesfeld. "Polymer electrolyte fuel cell model." *Journal of the electrochemical society* 138, no. 8 (1991): 2334.
- [36] Chorin, Alexandre Joel. "Numerical solution of the Navier-Stokes equations." *Mathematics of computation* 22, no. 104 (1968): 745-762.
- [37] Wang, Lin, Attila Husar, Tianhong Zhou, and Hongtan Liu. "A parametric study of PEM fuel cell performances." *International Journal of Hydrogen Energy* 28, no. 11 (2003): 1263-1272.